Brain Struct Funct (2007) 212:55–73
DOI 10.1007/s00429-007-0143-3

ORIGINAL ARTICLE

Morphological characterization of electrophysiologically and immunohistochemically identified basal forebrain cholinergic and neuropeptide Y-containing neurons

Alvaro Duque · James M. Tepper · Laszlo Detari · Giorgio A. Ascoli · Laszlo Zaborszky

Received: 22 March 2007 / Accepted: 2 May 2007 / Published online: 2 June 2007

Abstract The basal forebrain (BF) contains cholinergic as well as different types of non-cholinergic corticopetal neurons and interneurons, including neuropeptide Y (NPY) containing cells. BF corticopetal neurons constitute an extrathalamic route to the cortex and their activity is associated with an increase in cortical release of the neurotransmitter acetylcholine, concomitant with low voltage fast cortical EEG activity. It has been shown in previous studies (Duque et al. in J Neurophysiol 84:1627–1635, 2000) that in anesthetized rats BF cholinergic neurons fire mostly during low voltage fast cortical EEG epochs, while increased NPY neuronal firing is accompanied by cortical slow waves. In this paper, electrophysiologically and neurochemically characterized cholinergic and NPY-containing neurons were 3D reconstructed from serial sections and morphometrically analyzed. Cholinergic and NPY-containing neurons, although having roughly the same dendritic surface areas and lengths, were found to differ in dendritic thickness and branching structure. They also have distinct patterns of dendritic endings. The subtle differences in dendritic arborization pattern may have an impact on how synaptic integration takes place in these functionally distinct neuronal populations. Cholinergic neurons exhibited cortically projecting axons and extensive local axon collaterals. Elaborate local axonal arbors confined to the BF also originated from NPY-containing neurons. The presence of local axon collaterals in both cholinergic and NPY neurons indicates that the BF is not a mere conduit for various brainstem inputs to the cortex, but a site where substantial local processing must take place.

Keywords Dendritic morphometry · Three-dimensional reconstruction · Axon collaterals · Rat

Electronic supplementary material The online version of this article (doi:10.1007/s00429-007-0143-3) contains supplementary material, which is available to authorized users.

A. Duque
Department of Neurobiology, Yale University School of Medicine, New Haven, CT 06510, USA

J. M. Tepper · L. Zaborszky (✉)
Center for Molecular and Behavioral Neuroscience, Rutgers, The State University of New Jersey, Newark, NJ 07102, USA
e-mail: zaborszky@axon.rutgers.edu

L. Detari
Department of Physiology and Neurobiology, Loránd Eötvös University, Budapest 1117, Hungary

G. A. Ascoli
Krasnow Institute for Advanced Study and Psychology Department, George Mason University, Fairfax, VA 22030, USA

Introduction

The basal forebrain (BF) consists of a heterogeneous group of telencephalic structures including the septum, the vertical (VDB) and horizontal limbs (HDB) of the diagonal band of Broca, the substantia innominata (SI) and the ventral pallidum. This brain area is of wide clinical interest because some of its cell populations have been found to be severely affected in a number of neurological maladies such as Alzheimer's disease, Parkinson's disease and schizophrenia (Davies and Maloney 1976; Whitehouse et al. 1982; Bartus et al. 1986; Heimer et al. 1991; Geula and Mesulam 1994; Sarter and Parikh 2005).

Neurons in the rat BF areas are heterogeneous in terms of neurochemical content, electrophysiology, and morphology. Neurochemically two major groups are usually distinguished, cholinergic and non-cholinergic. The

non-cholinergic neurons are mainly GABAergic and have been shown to contain various calcium-binding proteins, including parvalbumin, calbindin and calretinin and various neuropeptides, including substance P, neuropeptide Y (NPY), somatostatin, enkephalin, neurotensin and galanin (Walker et al. 1989a, b; Pang et al. 1998; Zaborszky et al. 1999; Gritti et al. 2003). A considerable proportion of neurons (approx. 5–30%) is believed to be glutamatergic (Gritti et al. 2003; Hur and Zaborszky 2005). Less than 1% of the BF neurons have been reported to co-localize GABA and choline acetyltransferase (ChAT), the enzyme that synthesizes acetylcholine (Brashear et al. 1986; Fisher and Levine 1989).

In terms of electrophysiology, various behavioral states are associated with different cortical electroencephalographic (EEG) patterns. In anesthetized rats, BF neurons that have a higher firing rate during low voltage fast electrical EEG states are termed F cells, and cells whose firing rate increases during high amplitude, slow cortical EEG activity are termed S cells (Detari and Vanderwolf 1987; Dringenberg and Vanderwolf 1998). However, it is important to note that there is great diversity among F and S cells in terms of conduction velocity, spontaneous and evoked neural activity and correlation between EEG and unit activities, indicating that F and S cells are far from being homogeneous cell populations (Detari 2000). In addition, there are some BF neurons whose activities are unrelated to EEG cortical changes (Nunez 1996).

Morphologically, most cholinergic cells are large and multipolar with extensive dendritic fields. Non-cholinergic neurons vary extensively in soma shape, and dendritic and axonal characteristics. Of the several neurochemically distinct non-cholinergic populations the NPY neurons were selected to be compared morphologically to the cholinergic neurons because they not only have a very different neurochemical make-up but also represent cell types with clearly different electrophysiological properties: cholinergic cells are ''F'' type; NPY-neurons are ''S'' type (Duque et al. 2000). Similar to the ChAT cells, parvalbumin positive, putatively GABAergic neurons are also classified as ''F'' cells (Duque et al. 2000; Duque and Zaborszky 2006).

Acetylcholine and NPY have both been implicated in Alzheimer's disease therefore making BF cholinergic and NPY-containing neurons very attractive cellular populations for investigation and morphological analysis. BF cholinergic neurons have been implicated in a number of important cognitive processes such as learning, memory, attention and arousal and it has been hypothesized that dysfunction of the cholinergic neurons is responsible for the cognitive deficits associated with the aforementioned illnesses (Heimer et al. 1991; Voytko et al. 1994; Sarter and Bruno 1999). NPY is among the most abundant neuropeptides in mammalian brain (Allen et al. 1983; Chronwall et al. 1985; de Quidt and Emson 1986a, b) and it has been shown that NPY levels in the CSF are significantly reduced in Alzheimer's dementia (Edvinsson et al. 1993; Minthon et al. 1996). NPY neurons have been detected in BF areas where several NPY receptor subtypes are abundantly expressed (Wolak et al. 2003; Zaborszky and Duque 2003). NPY local injection into the BF resulted in a significant increase in relative delta power of the EEG and a decrease in theta, alpha and beta frequency bands (Toth et al. 2005).

Because of their distinct neurochemical make up, their opposite spontaneous activity in reference to cortical activity, and because morphology can affect cellular properties and function, we were interested in investigating if there are morphometric differences between cholinergic and NPY-containing BF neurons. In particular, since computational studies suggest that dendritic morphology can robustly affect neuronal electrophysiological properties (Carnevale et al. 1997; Schaefer et al. 2003), we studied dendritic numerical and topological features.

Materials and methods

Experimental animals

Male Sprague Dawley rats (n = 92; 250–350 g; Zivic Miller Laboratories, Inc, Portersville, PA) were housed two to a cage and allowed food and water ad libitum. All procedures described here were carried out in strict accordance with guidelines set forth in the PHS manual ''Guide for the Care and Use of Laboratory Animals'', conform to NIH guidelines and were approved by the Rutgers University Institutional Review Board. The electrophysiological and neurochemical identification of the neurons presented here has been previously published (Duque et al. 2000) hence, these aspects are only briefly mentioned here.

Anesthetics, surgical procedures and recordings

Rats were anesthetized with urethane (1.2 g/kg i.p. supplemented as necessary) and placed in a stereotaxic apparatus, skull adjusted to have lambda and bregma on the same horizontal plane. All wound margins and points of contact between the animal and the stereotaxic apparatus were infiltrated with lidocaine solution (2%) and xylocaine ointment (5%), respectively. Body temperature was kept at 37°C with an electric heating pad. The scalp and overlying fascia were reflected from the skull and small burr holes were drilled, in both hemispheres, over the pre-frontal/frontal cortex for EEG recordings. Simultaneous cortical EEG and single cell extracellular recordings from different

BF areas including the HDB, the SI or the ventral globus pallidus, were obtained. Following extracellular recordings, neurons were juxtacellularly labeled with 5% biocytin as described elsewhere (Pinault 1996; Pang et al. 1998; Duque et al. 2000; Duque and Zaborszky 2006). In 51 rats two cells were labeled, one cell per hemisphere. In 37 rats a single cell was labeled. In one case we had three cells in one hemisphere and one in the other hemisphere and in two cases we had one cell in one hemisphere and two in the other. Finally we had one case in which only two cells were labeled and they were in the same hemisphere. In all cases in which more than one cell was labeled in one hemisphere all the cells were F type and all were more than 800 μ apart in the rostrocaudal axis. Every neuron presented in this paper was the sole neuron juxtacellularly labeled in a hemisphere.

Perfusion, tissue processing and immunocytochemistry

At the completion of the experiment, rats were deeply anesthetized with urethane and perfused with 150–200 ml saline followed by 200 ml of 4% paraformaldehyde, 15% picric acid and 0.5% glutaraldehyde and then by 200 ml of the same fixative without glutaraldehyde. Brains were left overnight in the second fixative. Coronal 50 µm sections were cut through the forebrain with a Vibratome®1000 Classic (Warner Instruments, Hamden, CT). For visualization of juxtacellularly labeled single cells, sections were incubated overnight in avidin conjugated lissamine rhodamine (LR) (1:500; Jackson ImmunoResearch Labs, West Grove, PA). Biocytin filled neurons were identified with a Zeiss Axioplan microscope equipped with epifluorescence setup. If a cell was electrophysiologically identified as F type, the section containing its soma was tested for the presence of ChAT. On the other hand, if it was S type, the section containing its soma was tested for NPY. For ChAT a monoclonal rat anti-ChAT antibody was used (1:10; 2 days at 4°C; Boehringer Mannheim, Germany). For NPY a rabbit polyclonal antibody was used (Rabbit anti-NPY; 1:500; 2 days at 4°C; Peninsula Laboratories, Inc, Belmont, CA). Visualization of ChAT or NPY was done with a secondary antibody conjugated to fluorescein isothiocyanate [FITC conjugated goat anti rat/rabbit; 1:100; 4 h at room temperature (RT); Jackson ImmunoResearch Labs, West Grove, PA]. Finally, all the sections containing a biocytin-stained cell were developed using 3,-3′-diaminobenzidine tetrahydrochloride (DAB) as a chromogen intensified with nickel (Ni) with a modification of the protocol described by Horikawa and Armstrong (1988). Sections were first incubated in biotinylated peroxidase (1:200, ''B'' component of the standard Avidin–Biotin Peroxidase complex (ABC) kit, Vector Laboratories Inc, Burlingame, CA) for 2 h at RT and then for 20 min in 0.05% DAB with 0.038% nickel ammonium sulfate. H_2O_2 was added to the DAB/nickel solution to a final concentration of 0.01%, and the tissue was agitated for another 10 min. After Ni–DAB developing of series of sections containing single juxtacellularly labeled identified NPY or cholinergic neurons those sections were immunostained against ChAT using the same procedure as for single cell visualization but the series of sections were developed using DAB as chromogen. Triton was omitted from the incubation solutions.

After being reacted with the second DAB, sections were thoroughly rinsed in PB and osmicated in a solution containing 1% osmium tetroxide (Electron Microscopy Sciences, Fort Washington, PA) in phosphate buffered saline (PBS), for approximately 30–40 min. The tissue was dehydrated in an ascending series of ethanol (30–50–70–90–100%). Contrasting was done by treating the tissue with 1% uranyl acetate (Electron Microscopy Sciences, Fort Washington, PA) in 70% ethanol, for 30 min. Afterwards, the tissue was dehydrated with 1% propylene oxide (Electron Microscopy Sciences, Fort Washington, PA). Finally, the sections were infiltrated in durcupan (Fluka Chemie AG, Buchs, Switzerland) overnight and then flat embedded between liquid release agent-coated (Electron Microscopy Sciences, Fort Washington, PA) microscope glass slides and coverslips. Embedding for electron microscopy enhances the optical quality of the tissue, allows very clear morphological reconstruction of the single juxtacellularly labeled cell at the light microscopic level and will permit future EM studies of the material.

Data acquisition

Biocytin-stained neurons were reconstructed using Neurolucida® (Microbrightfield Inc, Williston, VT) interfaced to a Zeiss Axioplan microscope. Selected single labeled neurons were reconstructed from 50 µm serial sections. Bulk labeling of ChAT neurons (light brown, DAB developed) in the vicinity of single juxtacellularly labeled ChAT or NPY neurons (pitch black, Ni–DAB developed) did not interfere in any way with our ability to visualize and morphologically reconstruct single cells. The number of sections containing individual neurons varied from 22 to 140. Outlines of the sections, contours of structures and fiducial markers were drawn with a 5× Plan-NEOFLUAR objective lens. Somata, dendritic and axonal branches were traced with a 100×, oil immersion ACHROPLAN objective lens. For serial reconstructions each section was aligned to a common reference, e.g., the lowest midline point of the corpus callosum. Additional alignment was applied using the 2–4 point matching function of the Neurolucida® software. Shrinkage corrections were applied using Neurolucida®. Morphometric data were extracted using the Neurolucida® companion software, NeuroExplorer (Mi-

crobrightfield Inc, Williston, VT) and the freely available program L-Measure (Scorcioni and Ascoli 2001; http://www.krasnow.gmu.edu/L-Neuron).

NeuroExplorer formulae and definitions

Soma perimeter and area were taken at their maximum by plotting the soma surrounding at the focus level at which it appeared to be the largest.

Tree: branched structures such as dendrites are organized in a form known as a tree. A tree consists of all dendritic processes originating from the same dendritic stem that is connected to the soma. The starting point of a tree is called stem or root. Segments or branches are the parts of the tree that connect endings (terminations) or nodes.

Dendrogram is a stylized drawing of a branched structure, e.g., axon or dendrite. For dendrograms the origin of the tree in the dendrogram is plotted at the left and different branch orders extend to the right. Dendrograms such as those shown in Figs. 4 and 7 clearly demonstrate the number of trees that originate from the soma and their branching pattern.

Branch order. We used the centripedal (also known as centrifugal) ordering system in our analysis because this ordering system is particularly good at providing information about both topological distance and amount of branching in a tree. Order was defined in such a way that the proximal segment of an unbranched dendrite is order 1 (primary dendrite or dendritic stem). The daughter branches split off the order 1 branch at a point called a node and they are of order 2, and that way successively to the end of a structure. Alternate branch order schemes are compared in a supplementary figure.

Dendritic length. The actual lengths of the different branches were measured, and the total length (from the start of the process to each ending) and the length of each segment per dendritic order were calculated. The length from any point to any other point can be obtained and the program calculates length using vector summations in 3D. Total dendritic length was defined as the sum of the length values for all the branches of each order belonging to each process and the mean length was then the total length divided by quantity, where quantity is the number of branches belonging to each process at each branch order.

Surface area and volume. The start and end point of each line segment has a radius value determined by the size of the circular inset of the cross-hair cursor used when tracing. The surface area of each line segment was computed using these radii values and the length of each line segment in the mathematical formulae for the surface area of a shape known as a right frustrum. For instance, if R_1 is the radius at the start of a line segment and R_2 is the radius at the end of the line segment and L is the length of line segment. Then, the lateral surface area (LSA) and the volume (V) of the right frustrum are defined as:

$$\mathrm{LSA} = \pi(R_1 + R_2)\sqrt{(R_1 - R_2)^2 + L^2}$$

$$V = \frac{1}{3}\pi L(R_1^2 + R_1R_2 + R_2^2)$$

The *planar angle* was defined as the angle between a daughter branch and the parent branch. This angle is computed using rays drawn from the beginning of a branch to its node or ending. This angle is computed in the plane defined by the two rays and its value can extend from 0 to 180 degrees, with 0 degrees indicating the branch is a straight-line continuation of its parent.

Definitions used from *L*-measure

Power ratio is the sum of the two daughter diameters elevated to 1.5 divided by the parent diameter elevated to 1.5. The value, computed over all bifurcating branches, would be one for ideal electrotonic structures (Rall's power formula).

Bifurcation angle is the angle between the two daughters of a bifurcation, calculated based on their first tracing points.

Daughter diameter ratio is the ratio between the initial diameters of the two daughters of a bifurcation.

Partition (topological) asymmetry is the absolute difference between the numbers of terminals of the two subtrees of a bifurcation, divided by the number of terminals of the parent minus two. This value is zero for perfectly symmetric topological trees, and one for perfectly asymmetric ones.

Taper rate is defined as the difference between the branch ending and starting diameter, divided by the starting diameter, and is calculated separately for bifurcating and terminating branches.

Branch contraction measures the *tortuosity or meander* of the branches, defined as the ratio between the Euclidian and the path distances between the starting and ending points of each branch. Branch length and diameter are calculated separately for bifurcating and terminating branches.

Statistics, documentation

Statistical analyses were performed in Microsoft® Excel (1998 edition) or in Origin 6.0 (Microcal Software, Inc, Northampton, MA). Morphometric data were statistically characterized using neuron-, tree- or branch-based analysis. When appropriate, group measures were compared using non-parametric testing (Mann–Whitney) or ANOVA and

Bonferroni corrected as appropriate. Significance was declared at $P < 0.05$. Digital photographs were taken with an Olympus BX60F epifluorescence microscope equipped with a DCS-420 digital camera or with a Zeiss Axioskop epifluorescence microscope equipped with an AxioCam. The contrast of digital images was enhanced with Adobe® PhotoShop.

Results

From 151 biocytin filled neurons that were also electrophysiologically identified, 35 neurons were immunotested of which six were positive for ChAT and four were positive for NPY. Positive dual immunolabeling was only accepted in cases in which the biocytin-filled neuron was clearly and without doubt immunopositive for ChAT or NPY, and other immunopositive neurons in the neighborhood showed the known pattern of distribution. Three cells from each category were selected for morphometric analysis based on the quality of the material and the completeness of the staining. All cholinergic cells were electrophysiologically classified as F type and all NPY neurons as S type. For a complete electrophysiological description see Duque et al. (2000).

3D reconstruction of cholinergic neurons: general characteristics

Figures 1, 2, 3 illustrate projected images of 3D reconstructions of two cholinergic neurons and Fig. 4 displays the dendrograms of three selected cholinergic neurons. Figure 1a illustrates the stacked images projected in frontal plane of the reconstructed cholinergic neuron 062R. This neuron was located in the ventral part of the SI. Its cell body measured 19.9 × 17.3 μm (longest and shortest diameter) and had a surface area of 248.4 μm^2. The two primary dendrites (13 and 16 μm; see Fig. 4) each divide into two secondary branches of unequal length (18/54 μm; 8.5/43 μm). The secondary branches divide into short and long tertiary branches (51/143; 75/200 μm), which further divide into long fourth and fifth order branches. Higher order divisions gave rise to further unequal branches that are shorter than the tertiary or quaternary branches. While the primary and secondary branches are smooth, higher order branches are varicose. Spine-like appendages can be seen on some of the distal dendrites.

Figure 1d shows the same cholinergic neuron, rotated in space in order to best illustrate the trajectory of its main axon. The thick axon emerges from the dorso-lateral aspect of the cell body and bifurcates within 20 μm from it (filled arrowhead in Fig. 1). The main axon shaft gives rise to several thin axon collaterals. It first travels laterally and then returns to the level of the cell body to then continue towards the septum. The other branch also gives rise to a few thin axon collaterals and continues to the piriform cortex. An additional thin axon emerging from a more medial location of the cell body (open arrowhead in Fig. 1) gives rise to a massive network of axon collaterals occupying mostly a medial position from the cell body. The axon collateral network was visible only with the 100× objective and was clearly studded with many varicosities. In Fig. 1d only four representative hemicoronal sections are shown from 140 sections through which the neuron was traced. Figure 2 illustrates the two main axonal branches of the same neuron giving rise to terminal fields in the rostral part of the piriform cortex, mostly in layer 2 although some boutons are also seen in layer 3 (Fig. 2a), and in the medial septum (Fig. 2b), respectively. Although many varicosities can be observed in the terminal fields (panels 2A1′, 2A2′ 2B1′), varicosities were not seen en route to these terminal fields (panel 2C′).

Figure 3 shows the reconstruction of cholinergic neuron 116R, located in the ventral part of the SI. The cell body measured 25.4 × 17.1 μm and had a surface area of 287.0 μm^2. This neuron had four primary dendrites, and their secondary and tertiary branches are somewhat longer than in the case of cholinergic neuron 062R, resulting in a larger total dendritic length (Fig. 4). Also, there seem to be fewer varicosities along the dendrites. The axon emanated from the dorsal aspect of the cell body and was traced for 2 mm in the dorsal direction. Along the way several collaterals were issued that terminated in and around the dendritic arbor of this neuron. Cholinergic neuron 004R (Fig. 4c) was localized within the fibers of the internal capsule adjacent to the ventral part of the globus pallidus. Its soma measured 39.2 × 17.2 μm and had a surface area of 379.5 μm^2. It had three primary dendrites that divided in the usual short–long fashion, but altogether the neuron had fewer long secondary dendrites than the other two cholinergic neurons. On the other hand, there were more higher order small branches. Interestingly, the dendrites of this neuron stretch the longest up to 800 μm. Its local axonal arbor was obscured by fibers of the internal capsule; nevertheless the total length of local axon collaterals measured an astonishing 4.2 mm. For comparison of the dendritic arborizations of these three neurons, Fig. 4 depicts the dendrograms next to the schematic drawings of the corresponding neuron.

The three cholinergic neurons analyzed had a total of nine dendritic trees with an average total dendritic length per cell of 4,183 ± 620 μm and an average total dendritic surface area per cell of 12,809 ± 1,748 μm^2. Cholinergic neurons had an average of 37 ± 12 dendritic nodes and 41 ± 12 dendritic endings and occupied an average volume

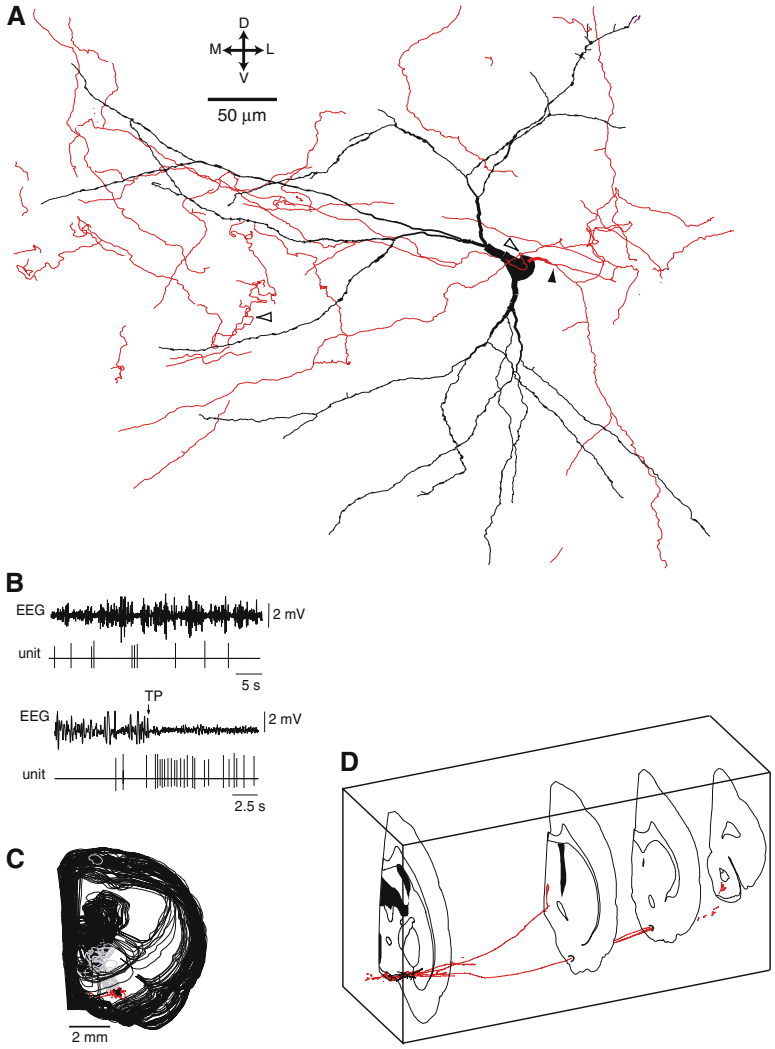

Fig. 1 **a** Neurolucida reconstruction of juxtacellularly labeled basal forebrain cholinergic neuron 062R. In this and all subsequent figures unless otherwise stated, the soma and dendrites are shown in *black* and the axon is shown in *red*. The distal main projection axon (*filled arrowhead*) was removed for better visualization of the extensive local axon collaterals (*open arrow-heads*). Abbreviations for topographical cross for this and all subsequent figures: *L*, lateral; *M*, medial; *V*, ventral; *D*, dorsal. **b** Concomitant unit and cortical EEG, spontaneous and tail pinch (*TP*) induced activity, demonstrating this cell is ''F'' type. See full electrophysiological analysis and neurochemical identification of all ChAT neurons presented here in Duque et al. (2000). **c** Some illustrative coronal section outlines (approximately 70 out of 140 serial sections) used in the reconstruction of this neuron. The removal of outlines is necessary to facilitate visualization of the neuron. **d** Schematic drawing showing this neuron slightly rotated in space to facilitate visualization of two axonal branches traveling rostrally. One of the branches travels medialwards and ends at the level of the septum. The other branch travels laterally and ends at the level of the rostral piriform cortex. For simplification only four hemicoronal outlines are shown. For illustration the axon terminals have been collapsed onto the corresponding representative hemicoronal outlines

of 3,753 ± 504 µm^3 per cell. Overall, dendritic endings had a tendency to terminate with a varicosity or bulge although sometimes from the varicose ending a short thin filopodium emanates.

As described, cholinergic axons gave rise to several collaterals bearing very fine en passant varicosities within a 0.2–0.3 mm^3 volume around the cell body. Although it was not possible to trace every single piece of axon due to lack of staining or other technical difficulties, the total lengths of cholinergic axon collaterals reconstructed were 3,260 µm (neuron 116R), 4,252 µm (neuron 004R) and 27,482 µm (neuron 062R).

3D reconstruction of NPY neurons: general characteristics

Figure 5a shows the reconstruction of NPY neuron 059R. This cell was located in the HDB. Its soma diameter measured 15.4 × 12.3 µm and it had a surface area of

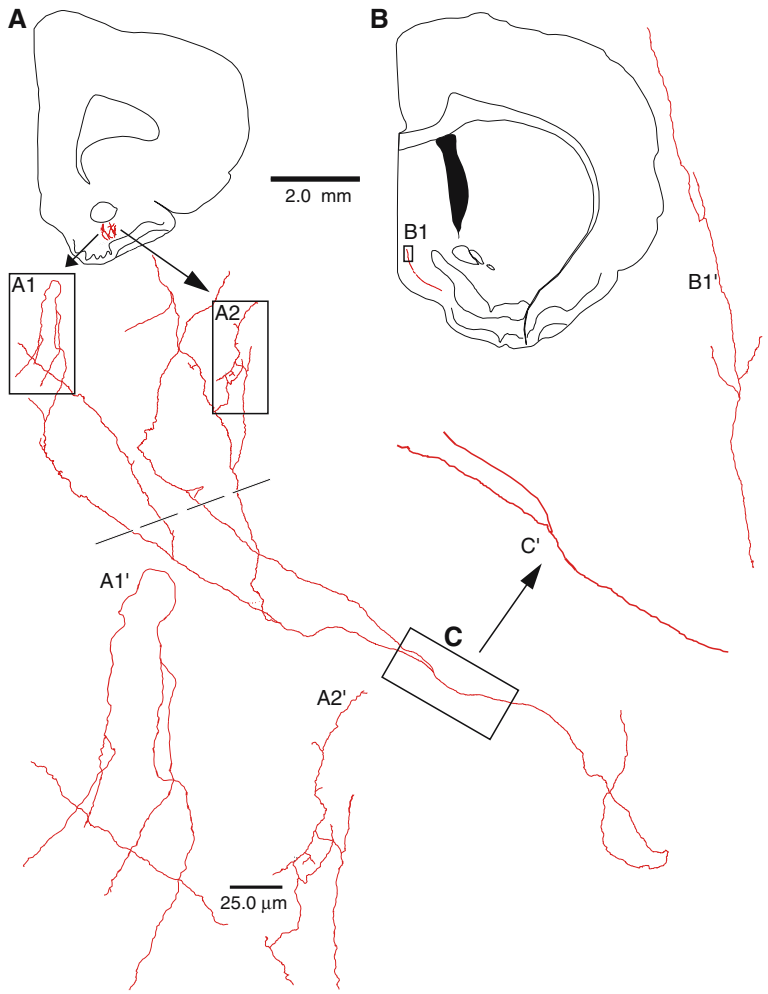

Fig. 2 Detailed view of cholinergic neuron 062R axon terminal field. **a** Details of the terminal field at the level of the rostral piriform cortex. For illustration some of the axon terminals in the area (up to the *dashed line*) have been collapsed into a single hemicoronal section. The *arrows* pointing out of the hemicoronal section indicate a magnified version of the axon. *Boxes* A1 and A2 enclosed axon areas that are again magnified at the lower left of the figure (A1′ and A2′). At this final level of magnification boutons are visible. **b** Details of the terminal field at the level of the medial septum. Here also the terminal field is not from a single coronal section but rather from several coronal sections collapsed into one for illustrative purposes. The axon in *box* B1 is magnified to the right of the figure so that boutons are visible (B1′). **c** illustrates axon en route to the rostral piriform cortex, hence it is continues with that shown in **a**. The magnification of the axon enclosed in **c**, shown immediately up and to the right of the *box*, indicates the absence of boutons (C′). Two millimeters scale bar applies to the hemicoronal sections shown in **a** and **b**. Twenty-five micrometers scale bar applies to the larger magnifications of the axon (A1′, A2′, B1′, C′)

129.8 µm^2. This neuron had five primary dendrites, four of which divided into ten relatively long dendrites (200–500 µm) that had several short side branches. The dendrites were somewhat wavy and moderately spiny. This neuron had a sizable local axon collateral arbor with 615 irregularly spaced small bouton-like varicosities that distributed mostly lateroventral to the position of the soma.

Figure 6a shows the reconstruction of NPY neuron 134R. The cell body measured 34.1 × 16.7 µm and had a surface area 307 µm^2. In this neuron, in addition to local collaterals, we found a thick projection axon that divided into two main branches one of which was lost from sight in the dorsal thalamus; the other branch was traced to near the stria terminalis at the edge of the lateral ventricle. Figure 6c shows this NPY neuron slightly rotated in space allowing a better angle that facilitates visualization of its projection axon. This neuron had five, relatively long primary dendrites (up to 300 µm) that divided into secondary and tertiary dendrites of various lengths. The primary and secondary dendrites were smooth with occasional spines. Most of the tertiary dendrites terminated in complex endings, often consisting of more than ten small spiny branchlets.

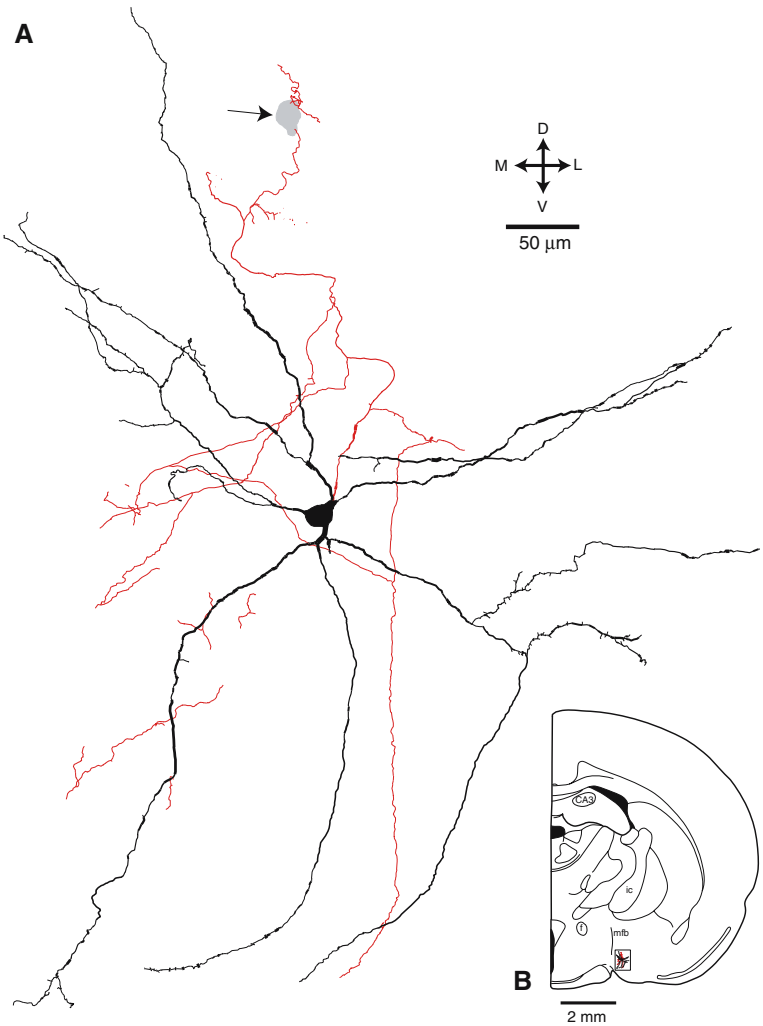

Fig. 3 **a** Neurolucida reconstruction of juxtacellularly labeled basal forebrain cholinergic neuron 116R. Not all the axonal arbor is shown. The *gray* profile indicated by the *arrow* represents another cholinergic neuron in close proximity to the reconstructed neuron's axon. *Inset* (**b**) indicates the location of this neuron in the ventral substantia innominata. *CA3*, hippocampus; *f*, fornix; *ic*, internal capsule; *mfb*, medial forebrain bundle

Figure 7 depicts the dendrograms next to the schematic drawing of the corresponding NPY-containing neurons. These three neurons had a total of 13 primary dendrites and two short (25–30 µm long) dendritic-like appendages emanating from the soma. The average total dendritic length per cell was 5,328 ± 2,285 µm and the average total dendritic surface area per cell was 14,468 ± 10,495 µm^2. NPY neurons had an average of 106 ± 93 dendritic nodes, 125 ± 112 dendritic endings and occupied an average volume of 4,061 ± 4183 µm^3.

Overall, dendritic endings had a tendency to terminate with a thin filopodial structure. However, it was noticed that most of the ventral sided dendritic terminals of NPY neuron 134R had racemose appendages, that is, twig-like branched dendritic appendages that contain varicosities, spines and some bulbous tips.

The axons of the NPY neurons also gave rise to several collaterals and although it was not possible to trace every single piece of axon due to lack of staining or technical difficulties, the total lengths of the axon collaterals from the NPY-containing neurons reconstructed were 1,796 µm (neuron 090R), 13,040 µm (neuron 059R) and 15,431 µm (neuron 134R).

Analysis of dendritic trees in cholinergic versus NPY-containing neurons

Table 1 lists and panels a–c in Fig. 8 display size- and topology related dendritic parameters. Panels d–f in Fig. 8 illustrate distribution morphometrics.

Dendritic thickness and length

There is no statistical difference in tree length (L_{ChAT} = 1,458 ± 596 mm; L_{NPY} = 1,294 ± 606 mm; P > 0.5, 2-tailed t test) or stem diameter (D_{ChAT} = 2.39 ± 1.57 mm; D_{NPY} = 2.01 ± 1.07 mm; P > 0.5) between the two groups (Table 1). Figure 8a illustrates that there is a difference in the mean dendritic diameter or thickness per branch order between the two populations. Across all dendritic orders, the mean diameter of the cholinergic

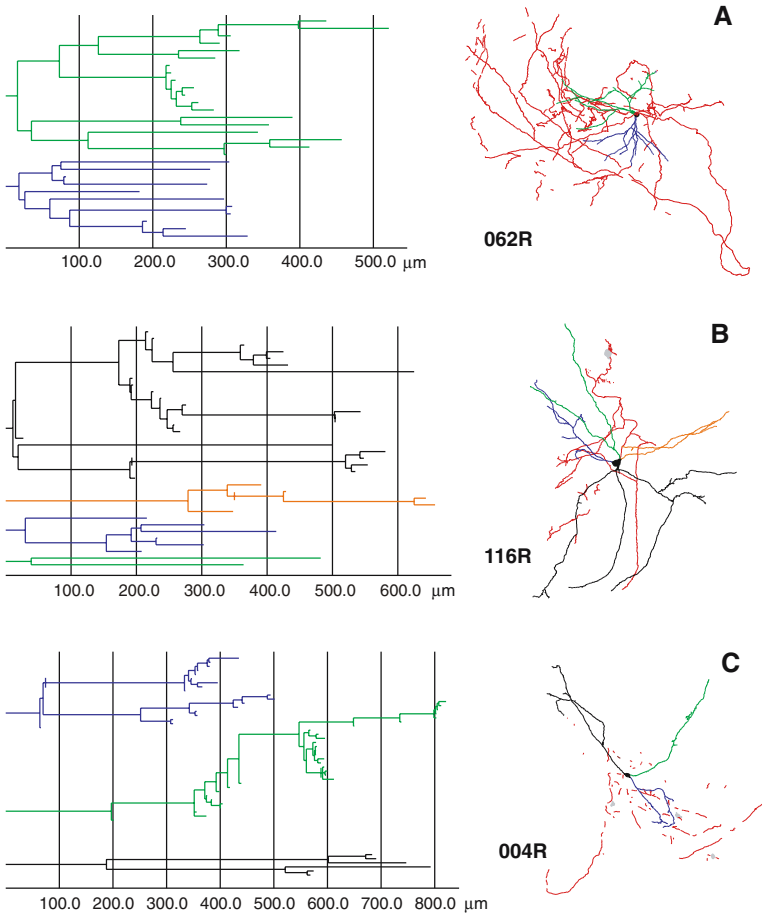

Fig. 4 Dendrograms of three cholinergic neurons. Neurons (not to scale) are shown on the *right* and the corresponding dendrograms on the *left*. The different dendrites in each neuron have been drawn in a different color, which corresponds to the branch color in the dendrogram. Somata are *black* and axons are *red*. **a** Cholinergic neuron 062R, **b** cholinergic neuron 116R. **c** Cholinergic neuron 004R. Note that as compared to Fig. 1a, the distal portion of the projection axon of the cholinergic cell 062R is included

dendrites is 0.967 ± 0.523 µm (n = 232 dendritic segments) while that of the NPY dendrites is 0.829 ± 0.381 µm (n = 691 dendritic segments). The difference between these means is statistically significant ($P < 0.0001$, 2-tailed Mann–Whitney test). If higher order branches are disregarded with the argument that they may simply be the result of small branchlets that should not be consider dendrites on their own right, and only the average diameter of primary, secondary, tertiary and quaternary dendrites was analyzed, the difference in average dendritic thickness is still statistically significant (n = 212 dendritic branches, $P < 0.0001$, 2-tailed Mann–Whitney test; see Table 1). Figure 8c shows the analysis of terminal and internal dendritic branch lengths in cholinergic and NPY neurons. Both terminal and internal branches are significantly longer in cholinergic than in NPY neurons. In addition, terminal branches are significantly shorter than internal branches in NPY (but not cholinergic) neurons (all P values are 2-tailed t tests).

Topology-related parameters

The number of dendritic orders was vastly different between the two chemically distinct neuronal populations as shown in Fig. 8a, b which indicates that while cholinergic dendrites run up to order 14, NPY dendrites run up to order 27. This simply means that NPY dendrites branch much more than cholinergic ones. This results from the fact that many small dendritic branchlets come out of main dendritic shafts especially towards the end field of dendrites (see dendrograms). These branchlets are morphologically distinct from spines and are in general longer than 5 μ. Hence, overall, the amount of branching of the NPY neurons roughly doubles the amount of branching of cholinergic neurons, and the main difference in branching is found towards the ends of dendrites. Dendrites of NPY positive neurons branch more than cholinergic dendrites at every order. This difference was statistically significant ($P < 0.05$, 2-tailed Mann–Whitney test). This indicates that even in the case of the most proximal dendrites, NPY dendritic trees branch more than cholinergic trees. This is not surprising since we noticed that at the root (soma) itself, the three cholinergic cells had nine primary dendrites and the three NPY neurons had 13 primary dendrites and two short (25–30 µm long) dendritic-like appendages.

Analysis of the planar angle of the branching dendrites, per dendritic order indicated that across all orders the mean branching angle of cholinergic dendrites was

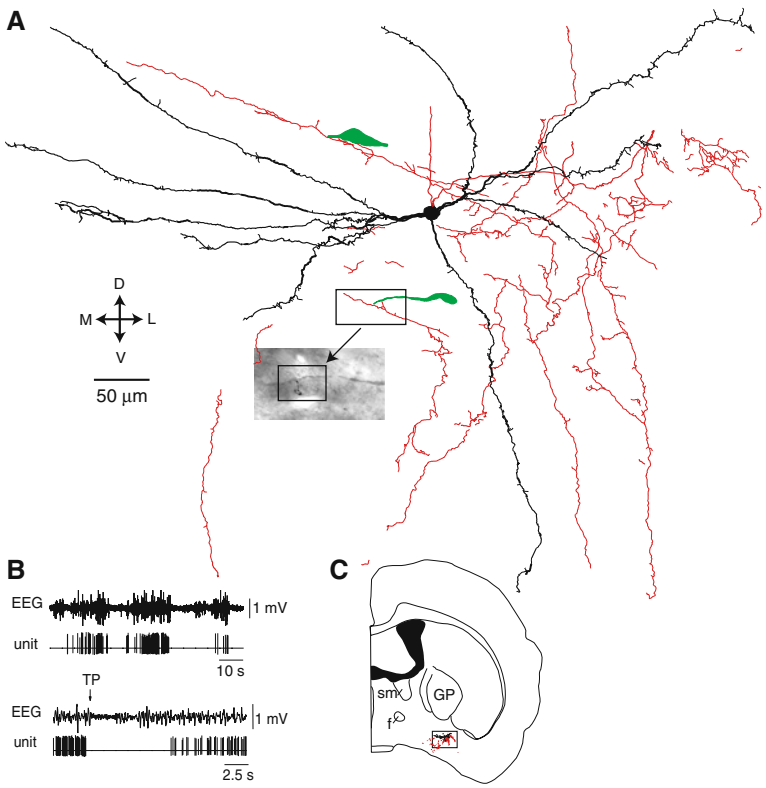

Fig. 5 **a** Neurolucida reconstruction of juxtacellularly labeled basal forebrain NPY positive neuron 059R. *Green* profiles are cholinergic neurons in close proximity to NPY axons. *Inset* shows possible contact site between NPY axon and cholinergic dendrite. **b** Concomitant unit and cortical EEG spontaneous and tail pinch (*TP*) induced activity demonstrating this cell is ''S'' type. See full electrophysiological analysis and neurochemical identification of all NPY neurons presented here in Duque et al. (2000). **c** Hemicoronal section indicating the position of this neuron in the horizontal limb of the diagonal band of Broca. *f*, fornix; *GP*, globus pallidus; *sm*, stria medullaris

56.5 ± 14.0 degrees while the average branching angle of NPY dendrites was 61.62 ± 7.69 degrees, this difference was not statistically significant. Similarly, there was no difference in the local bifurcation angle between the two daughter branches of a bifurcation. There was no difference in the measure of branch tortuosity between cholinergic and NPY neurons; however, NPY neurons show significantly larger topological (partition) asymmetry than cholinergic neurons. In the taper rate a substantial difference was found between bifurcating and terminating branches, but not between cholinergic and NPY neurons (Table 1).

Distribution morphometrics were obtained by looking at the distributions of scalar morphometrics as a function of dendritic path distance from the cell body. The distribution of membrane surface as a function of the distance from the soma along the dendritic path is illustrated in Fig. 8d. Accordingly, the distribution of surface area is concentrated closer to the soma in cholinergic than in NPY neurons. Figure 8e shows that if each of the six neurons were ''scaled'' to the same size, the dendritic surface area would have very similar distribution along the dendritic path in both ChAT and NPY neurons, thus the shift of the curve for NPY neurons in Fig. 8d reflects simple scaling rather than difference in the intrinsic structure of the dendrites.

The relationship between total dendritic tree length and stem diameter (the start diameter of the primary dendrite) in cholinergic (n = 9 trees, black symbols and lines) and NPY (n = 13 trees, red symbols and lines) neurons was also investigated as illustrated in Fig. 8f. A strong linear correlation is observed between the two measures in both groups (R_{ChAT} = 7.2, R_{NPY} = 7.6). However, the linear relationship between length and diameter has different characteristics in the two cell groups (the intercept is twice as big in cholinergic vs. NPY neurons). For example, an NPY tree with a stem of 4 µm is expected to be 250% longer than an NPY tree with a stem of 1 µm. In contrast, a ChAT tree with a 4 µm stem would only be expected to be less than 50% longer than a ChAT tree with a 1 µm stem.

Discussion

The main findings of this study are: (1) cholinergic and NPY-containing BF neurons have roughly the same dendritic surface areas and lengths but differ in dendritic branching, dendritic thickness and pattern of dendritic endings; (2) both cholinergic and NPY-containing neurons emit local axon collaterals.

Technical considerations

Juxtacellular labeling, neuron reconstruction. The six neurons morphologically analyzed in detail for this study were all juxtacellularly labeled and reconstructed by the

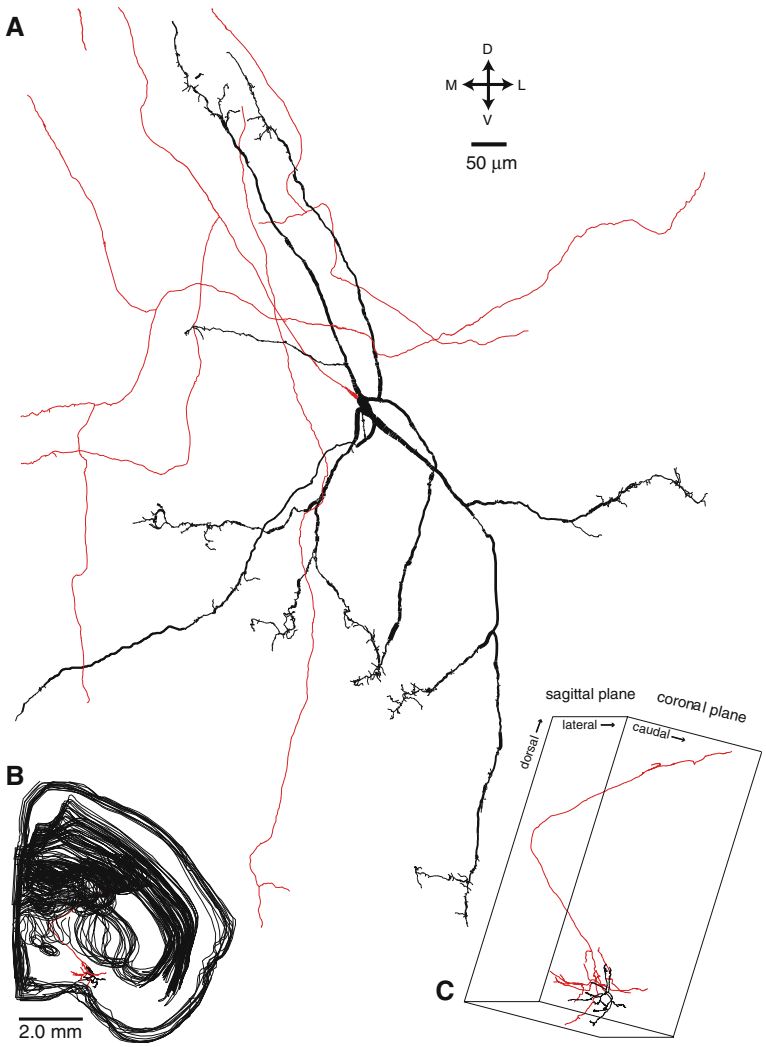

Fig. 6 **a** Neurolucida reconstruction of juxtacellularly labeled basal forebrain NPY positive neuron 134R. Not all of the axonal arbor is seen here since the main projection axon was removed for better visualization of the local axon collaterals. Notice that most of the dendritic endings are very complex. **b** Illustrative coronal sections from the serial reconstruction of this neuron. Several outlines have been either removed or made thinner to allow visualization of the neuron. The projection axon was artificially made thicker for easier viewing. **c** View of this neuron slightly rotated in space showing the axon traveling dorsally, rostrally and then caudally

same person using the same Neurolucida® system. Except for different immunoreagents, all material was essentially treated in the same way. Thus, the detected morphological variability between NPY and cholinergic neurons is more likely to reflect true differences instead of treatment or operator artifacts. This is important in view of the fact that significant morphometric differences have been found between reconstructions of the same material by two different operators using the same system (Jaeger 2001) and even by the same person when using two different reconstruction systems (Kaspirzhny et al. 2002). In a quantitative study of hippocampal pyramidal cells statistically significant differences were not only found between anatomical classes (CA3 vs. CA1 pyramidal cells), but also in the same morphological class when neurons were reconstructed in different laboratories (Scorcioni et al. 2004). Although juxtacellular labeling can produce ''Golgi like'' staining (Pinault 1994), the recording and labeling technique has some limitations, most importantly, that the quality of the fill depends on the length of time the cell is entrained for and might not be as complete as the filling with intracellular techniques if the cell is not labeled long enough. However, this is a limiting factor that affects mostly, in our experience, axonal labeling but does not affect in any significant way the high quality dendritic labeling that was required for this study.

Branch ordering. The high numbers for dendritic orders may appear artificial but they are a direct consequence of the centrifugal (or centripedal) ordering scheme that was chosen precisely because of its ability to detect amount of branching (see Supplementary Fig. 1). According to this method the program counts the distance from the root in terms of the segments traversed. Any missing portion of the tree does not result in incorrect numbering of known segments. The method is independent of the distribution of branches (whether or not a tree is balanced) and provides general topological parameters. The centripete (retrograde maximal ordering, diameter or Horsfield order), terminal

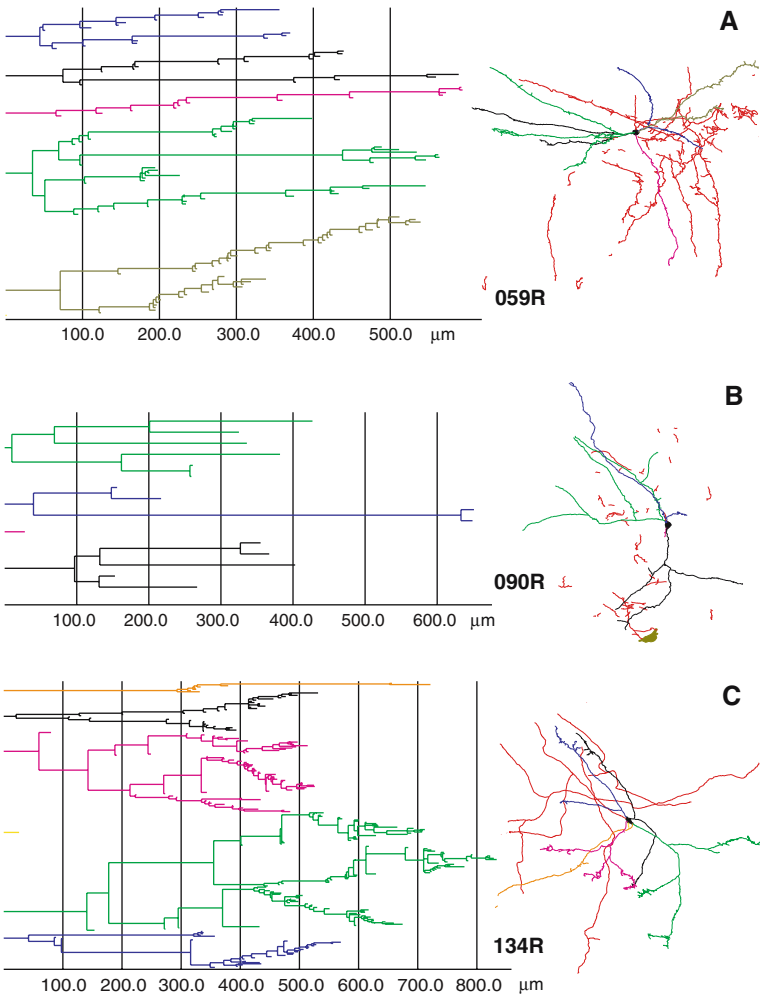

Fig. 7 Dendrograms of three NPY positive neurons. Neurons (not to scale) are shown on the *right* and the corresponding dendrograms on the *left*. The different dendrites in each neuron have been drawn in a different color, which corresponds to the branch color in the dendrogram. In all cases somata are *black* and axons are *red*. **a** NPY neuron 059R. **b** NPY neuron 090R. The *green profile* at the bottom represents a cholinergic cell body in close proximity to the reconstructed neuron. **c** NPY neuron 134R. The two short dendritic like appendages originating from the cell body of neuron 090R and neuron 134R (*short yellow lines*) in **b** and **c** are included in the dendrogram

distance (retrograde minimal ordering) and Strahler ordering methods begin labeling at the terminals and work the ordering towards the root. For our interests the Strahler system has the drawback of not counting a topological distance property and is affected by balance. The terminal distance method has the drawback of missing information on the amount of branching (see Supplementary Fig. 1). Obviously, the method of choice affects the number of branch orders. For example, using the Strahler method, all three cholinergic neurons have four dendritic orders, while the number of orders in case of the NPY neurons varies between three and five. If instead of the Strahler method, one would apply the centripete ordering scheme then the average number of dendritic orders for the three cholinergic neurons is ten and that for the three NPY cells is 17.6. Using the terminal distance type of ordering ChAT cell #062 has six orders but NPY neuron #134 runs only to order 2 giving a totally wrong impression of the extent of branching. However, one has to bear in mind that the extraction of measures like terminal versus internal branch length, partition asymmetry, diameter of dendrite stem is independent of the branch ordering scheme used.

Statistical considerations. Since we have detailed morphological parameters for only three neurons per group, we cannot perform statistics on cell body measures (perikaryon volume, surface, etc.) and no statistical differences were found if we applied tree-based analysis (see first 8 values in Table 1 and Fig. 8e) though we found significant differences in comparing the number of dendritic branches per dendritic order between ‘‘average’’ NPY and cholinergic neurons using the centripedal branch order scheme (Fig. 8b). Since each neuron provides a large number of dendritic segments, branch-based analysis as opposed to tree-based or neuron-based allows very reassuring statistical power and, indeed, we found significant differences in measures, including terminating versus bifurcating branch length, topological asymmetry and dendritic diameter between NPY and cholinergic neurons (lines 17–18, 21 and 9 in Table 1). Even if dendritic branches are not absolutely independent observations, the results of this analysis reflect a trend that does have biological meaning. An important limitation of the present study is that it is based on only six fully reconstructed electrophysiologically and neurochemically identified cells. Therefore whether or not cholinergic

Table 1 Comparison of dendritic morphometric data between ChAT and NPY neurons

	ChAT	NPY
Total dendritic length/cell	4,183 ± 620	5,328 ± 2,285
Dendritic surface/cell	12,809 ± 1,748	14,468 ± 10,495
Dendritic volume/cell	3,753 ± 504	4,061 ± 4183
Number of nodes/cell	37 ± 12	106 ± 93
Number of endings/cell	41 ± 12	125 ± 112
Number of trees/cell	3 ± 1	4.33 ± 1.15
Max branch order/cell	14	27
Dendritic tree length	1,458 ± 596	1,294 ± 606
Dendritic diameter across all orders	0.967 ± 0.523[a]	0.829 ± 0.381[a]
Initial diameter of dendrite stem	2.39 ± 1.57	2.01 ± 1.07
Diameter, primary	2.19 ± 1.36[a]	1.50 ± 0.62[a]
Diameter, secondary	1.46 ± 0.74[a]	1.04 ± 0.50[a]
Diameter, tertiary	1.13 ± 0.37[a]	0.87 ± 0.39[a]
Diameter, quaternary	0.96 ± 0.31[a]	0.84 ± 0.38[a]
Power ratio	1.59 ± 1.74	1.36 ± 0.87
Daughter diameter ratio	2.36 ± 1.89	2.77 ± 1.54
Terminating branch length	48.93 ± 92.29[b]	13.22 ± 29.92[b,d]
Bifurcating (internal) branch length	65.31 ± 86.70[c]	33.09 + 57.33[c,d]
Planar angle across all orders	56.5 ± 14.0	61.62 ± 7.69
Local bifurcation angle	92.29 ± 35.16	90.34 ± 37.97
Topological (partition) asymmetry	0.57 ± 0.46[e]	0.79 ± 0.38[e]
Bifurcation branch taper	–0.06 ± 0.80[f]	–0.01 ± 0.55[g]
Terminating branch taper	–0.30 ± 0.54[f]	–0.23 ± 0.59[g]
Bifurcating branch tortuosity	0.81 ± 0.14	0.79 ± 0.18
Terminating branch tortuosity	0.83 ± 0.14	0.79 ± 0.16

[a] Statistically significant (Mann–Whitney *U* test)

[b–g] Statistically significant (2-tailed Bonferroni corrected)

and NPY neurons would show significant differences in measures in which we did not find them in this study awaits further investigations using a larger pool of neurons similarly identified.

Dendritic arborization pattern of cholinergic and NPY neurons

In agreement with dendritic morphology of physiologically identified putative cholinergic neurons of the laterodorsal tegmental nucleus (Surkis et al. 1996), the dendrites of BF cholinergic and also of NPY neurons resemble to some extent those of the ''isodendritic core'' (Ramon-Moliner and Nauta 1966) or generalized type of dendritic arbor (Scheibel and Scheibel 1961; Valverde 1961a, b; Ramon-Moliner 1962; Leontovich and Zhukova 1963; Brauer et al. 1988; Pang et al. 1998) of neurons in the reticular formation of the brainstem. For e.g., the presence of few, relatively straight dendrites and a branching pattern of cholinergic and NPY dendrites in which the sum of the lengths of the daughter branches is longer than the length of the parent branch is consistent with this classification. According to our estimates one cholinergic cell dendritic domain might share its space with 50–80 other cholinergic neurons, depending on its location in the BF, a characteristic of isodendritic neurons. This assessment is more difficult to do for NPY neurons, whose detection may depend heavily on the methodological approach. In colchicine pretreated animals, with excellent staining of the NPY somata and dendrites, the dendritic domain of a single NPY neuron may be shared with 5–15 other NPY neurons (Zaborszky and Duque 2000, 2003). However, there are some differences between these two types of neurons. For example, in NPY neurons short dendritic-like appendages emanating from the soma were common. Also, the claw-like (racemose) dendritic endings of NPY neuron 134R are similar to the complex dendritic appendages of some pallidal neurons described by Millhouse (1986) and are not encountered in cholinergic neurons. NPY dendritic trees are significantly more asymmetric than those of cholinergic neurons (partition asymmetry is 0.79 for NPY and 0.56 for cholinergic dendritic trees). Other cell classes have asymmetry values consistent with ChAT cells rather than NPY neurons, including spinal motoneurons at 0.46 ± 0.05 (Li et al. 2005) and hippocampal pyramidal cells at 0.54 ± 0.06 (Scorcioni et al. 2004), suggesting that highly asymmetric dendrites may be a specific peculiarity of NPY cells. Comparing data of bifurcation angle, branch tortuosity, and daughter diameter ratio, in contrast, did not reveal any statistically significant difference between NPY and ChAT neurons nor between either of these and hippocampal pyramidal or spinal motor neurons (Scorcioni et al. 2004; Li et al. 2005).

Both types of dendritic trees arborize in a box of about 0.1 mm^3; hence the actual space occupied by dendrites corresponds only to a fraction of their total spatial domain. There was no significant difference in total dendritic length comparing the average total dendritic length per cell type (n = 3 for ChAT and n = 3 for NPY), or the average total length per dendritic tree of each neuron type (n = 9 for ChAT neurons and n = 13 for NPY-containing neurons, without the small dendritic like appendages emanating from the soma). It should be noted that these dendritic length values are substantially lower that those reported for hippocampal pyramidal cells (16 ± 6 mm in Scorcioni et al. 2004) and spinal motoneurons (15 ± 6 mm in Li et al. 2005). In addition, in pyramidal and motor neurons length values are similar for bifurcating and terminal branches. In BF neurons, as illustrated in Fig. 8c, both terminal and

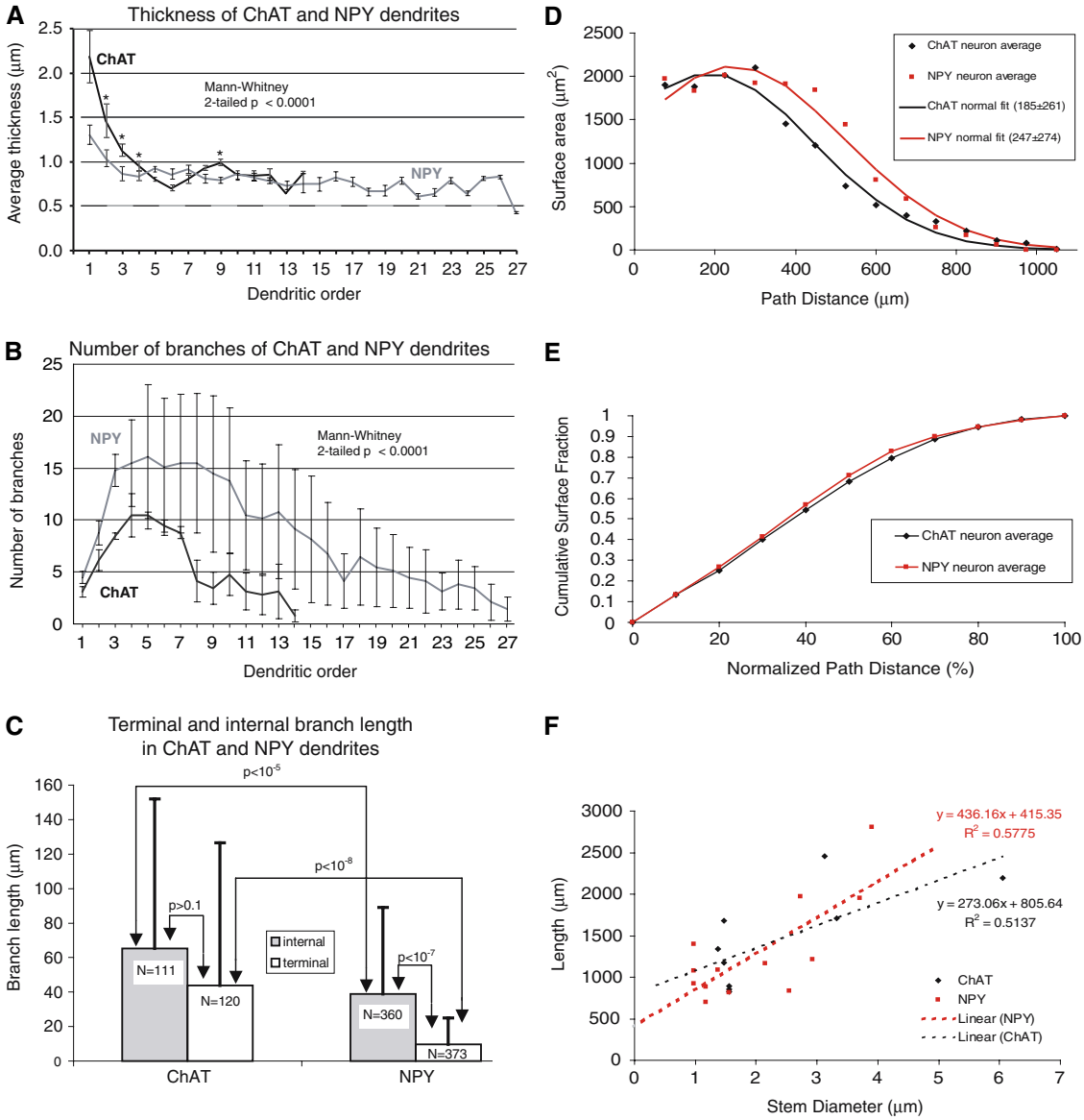

internal branches are significantly longer in cholinergic than in NPY neurons and terminal branches are significantly shorter than internal branches in NPY (but not ChAT) neurons. Interestingly, the initial (stem) diameter of the tree is a stronger predictor of dendritic length in NPY than in ChAT neurons (Fig. 8f).

Dendritic morphology and structure–function relationship

A major function of dendrites, assuming only passive behavior, is to collect synaptic input and deliver an electrotonically integrated version to the soma and down the axon initial segment where output action potentials are generated. Mounting evidence from computational studies suggests that dendritic morphology can robustly affect electrotonic properties (Carnevale et al. 1997), firing patterns (Krichmar et al. 2002), synaptic integration (Poirazi et al. 2003) and coincidence detection (Schaefer et al. 2003). The electrotonic structure of dendrites has been shown to play a critical role in neuronal computation and plasticity and some effort has been made to construct morphoelectrotonic transforms (a graphical mapping from morphological into electrotonic space) that would provide a way for rapidly obtaining information on the functional properties of dendritic trees (Zador et al. 1995; Carnevale et al. 1997). Propagation of action potentials in dendrites has also been shown to depend on dendritic morphology; simulations performed with reconstructions of different neuronal types demonstrated that the range of action potential back-propagation efficacies observed experimen-

◀ **Fig. 8** **a** Dendritic diameter versus branch order. Cholinergic dendrites, in *black*, run up to order 14. NPY dendrites are in *gray* and run up to order 27. The *y* axis corresponds to the average of the average diameter of dendrites for each order and is given in μm. There is a difference in the mean dendritic diameter or thickness per branch order between the two populations. Across all dendritic orders, the mean diameter of the cholinergic dendrites is 0.967 ± 0.523 μm (n = 232 dendritic segments) while that of the NPY dendrites is 0.829 ± 0.381 μm (n = 691 dendritic segments). The difference between these means is statistically significant ($P < 0.0001$, 2-tailed Mann–Whitney test). **b** Average number of branches per dendritic order for cholinergic and NPY basal forebrain neurons. The plot indicates that in general, cholinergic neurons have fewer branches than NPY neurons at every dendritic order. Data were normalized by the number of neurons, so that the data correspond to an ''average'' neuron of a particular type, i.e., cholinergic or NPY. Cholinergic data are in *black* and NPY data in *gray*. The number of dendritic orders was vastly different between the two chemically distinct neuronal populations. Overall, dendrites of NPY positive neurons branch more than cholinergic dendrites at every order. This difference was statistically significant ($P < 0.05$, 2-tailed Mann–Whitney test). **c** Terminal and internal branch lengths in ChAT and NPY neurons. Both terminal and internal branches are significantly longer in ChAT than in NPY neurons. In addition, terminal branches are significantly shorter than internal branches in NPY (but not ChAT) neurons (all P values are 2-tailed t tests). **d** Distribution of membrane surface along the dendritic path. In absolute terms, the distribution of surface area is concentrated closer to the soma in ChAT than in NPY neurons, although the total amount of surface is approximately the same in the two neuronal groups. **e** Cumulative surface fraction as a function of normalized path distance indicates that if each of the six neurons was ''scaled'' to the same size, then, the dendritic surface area would have very similar distribution along the dendritic path in both ChAT (N = 9 trees, *black symbols* and *lines*) and NPY (N = 13 trees, *red symbols* and *lines*) cells. **f** Plotting dendritic length as a function of stem diameter indicates a strong linear correlation (*dashed lines*) between the two measures in both groups (R_{ChAT} = 7.2, R_{NPY} = 7.6), and there is no statistical difference in tree length (L_{ChAT} = 1,458 ± 596 μm; L_{NPY} = 1,294 ± 606 μm; $P > 0.5$, 2-tailed t test) or stem diameter (D_{ChAT} = 2.39 ± 1.57 μm; D_{NPY} = 2.01 ± 1.07 μm; $P > 0.5$) between the two groups. However, the linear relationship between length and diameter has opposite characteristics in the two groups: the *intercept* is nearly twice as large for ChAT than for NPY neurons (In ChAT = 806 μm vs. In NPY = 415 μm), while the slope follows the opposite inequality (Sl_{ChAT} = 273 vs. Sl_{NPY} = 436), indicating a stronger dependence of total length on stem diameter for NPY than for ChAT dendritic trees

tally could be reproduced by variations in dendritic morphology alone (Vetter et al. 2001). Computational models of neuronal firing using 3D reconstructions of dendritic morphology (of hippocampal cells) found that differences between anatomical classes and within the same morphological class can have a dramatic influence on firing rate and mode (Krichmar et al. 2002; Scorcioni et al. 2004). There is no significant difference in the ''power ratio'' between the two classes of BF neurons examined here, as well as between either NPY or ChAT (Table 1) and either hippocampal pyramidal cells (at 1.7 ± 0.1 in Scorcioni et al. 2004) or spinal motoneurons (at 1.4 ± 0.2 in Li et al. 2005). Since the power ratio measures the deviation from ''ideal'' cable behavior, it is inviting to speculate that, in the assumption of similar electrotonic characteristics, the passive integrative/coincidence detection properties of ChAT and NPY cells may be comparable. However, the differences in branching patterns and branch-level morphometry (Fig. 8c, f; Table 1) combined with potential differences of active properties could enable and implement distinct dynamics and functions between the two neuronal types (Vetter et al. 2001; Krichmar et al. 2002; Schaefer et al. 2003). Some of the active dendritic conductances of cholinergic neurons in BF slices have been characterized (Khateb et al. 1992; Alonso et al. 1996), but no such data are available for NPY neurons in the BF.

If the length and surface area of the dendrites are an indication of the possible number of incoming inputs, then based on the results presented here, both cholinergic and NPY-containing BF neurons may receive roughly the same overall number of synapses. However, cholinergic neurons with more surface area in the very proximal dendrites might receive more inputs there than NPY neurons. Although some distal portions of cholinergic dendrites are thicker than distal endings of NPY dendrites, the complex endings of NPY dendrites with their increased surface area may compensate for their thinner proximal dendrites.

Increase in dendritic branching and length in BF neurons has been described in Alzheimer's disease using the Golgi method that non-specifically labels all types of neurons (Arendt et al. 1986). Our study is the first attempt at creating a basic set of dendritic parameters for specific neuronal types in the BF against which alterations can be measured in pathological conditions.

Local axonal collaterals of cholinergic and NPY-containing BF neurons

Using Golgi impregnation or ChAT immunostaining (Brauer et al. 1988), only the initial portions (up to 50 μm) of the axons can be observed and hence these methods are not useful in observing axon collaterals.

Searching for contacts from putative cholinergic collaterals onto GABAergic parvalbumin-immunoreactive rat medial septum neurons, Brauer et al. (1998) injected the immunotoxin 192IgG-saporin into the septal diagonal band region and reported, at the EM level, degenerating terminals in contact with both parvalbumin positive and negative cells. Since the immunotoxin is supposed to affect only cholinergic cells (Book et al. 1994), it was deduced that local cholinergic collaterals must be present in the region, a suggestion in agreement with previous presumptions to the effect (Bialowas and Frotscher 1987). However, cholinergic collaterals were not directly demonstrated.

A study using intracellular injection of HRP for staining of antidromically identified neurons revealed that

corticopetal neurons in the BF had local axon collaterals displaying numerous boutons en passant (Reiner et al. 1987; Semba et al. 1987). However, due to the lack of transmitter identification, the classification of the reconstructed neurons remained open to speculation (Detari et al. 1999). A patch clamp study by Bengtson and Osborne (2000) shows a reconstructed cholinergic neuron in the ventral pallidum, which does not seem to have axon collaterals (although a small daughter branch is reported). However, this was an in vitro study where truncation of axons and dendrites is very common. A study of juxtacellularly labeled cholinergic neurons in the BF by Manns et al. (2000) did not describe the axons of the labeled neurons. In our study all cholinergic neurons reconstructed possessed axon collaterals. To our knowledge this is, therefore the first time that local axon collaterals of BF cholinergic neurons have been demonstrated.

Several studies in brain slices containing the septum and diagonal band have documented that cholinergic neurons are capable of releasing acetylcholine locally in an impulse dependent manner (Metcalf et al. 1988; Metcalf and Boegman 1989; Nishimura and Boegman 1990), a finding that is in agreement with the presence of abundant local axonal collaterals of cholinergic neurons shown in this study. Moreover, both nicotinic and muscarinic receptors are found in the BF (Yu et al. 1993; Vilaro et al. 1994; Gotti et al. 1997; Khateb et al. 1997, 1998; Csillik et al. 1998; Jones and Muhlethaler 1999; Smiley et al. 1999a, b; Picciotto et al. 2000; Dani 2001). Muscarinic inhibition of glutamatergic transmission onto rat magnocellular BF neurons has been seen in slice preparations (Sim and Griffith 1996). Cholinergic neurons have been shown to be hyperpolarized by muscarine (Khateb et al. 1997) and muscarinic receptor agonists strongly excite non-cholinergic, presumably GABAergic neurons in BF slices (Wu et al. 2000), findings that are compatible with the idea that cholinergic neurons may influence other local cholinergic, glutamatergic and GABAergic neurons.

Although NPY axons have been shown to synapse with cholinergic neurons in the BF using bulk-immunostained material (Zaborszky and Duque 2000), due to the fact that NPY is expressed in most of the brainstem catecholaminergic neurons with ascending projections to BF cholinergic neurons (Zaborszky and Cullinan 1996; Hajszan and Zaborszky 2002), the local origin of NPY synapses on cholinergic neurons cannot be ascertained by these studies. On the other hand, reconstruction of the local axon-collaterals of NPY neuron #059 from ultrathin sections, indeed confirmed, in preliminary studies, that NPY varicosities establish synapses with cholinergic dendrites (Mosca et al. 2005). Since in the axonal arborization space of a single NPY neuron, in addition to cholinergic neurons a large number of other types of neurons exists, including various calcium-binding protein containing neurons (Zaborszky et al. 2002), the local postsynaptic targets of the NPY axons remain to be established in future electron microscopic studies. NPY is colocalized with GABA (Aoki and Pickel 1989) and/or somatostatin (Köhler et al. 1986) in many forebrain neurons. NPY has been shown to inhibit GABA release presynaptically in isolated self-innervating suprachiasmatic neurons (Chen and Van den Pol 1996) and mediate postsynaptic dendritic hyperpolarization in the thalamus (Sun et al. 2001, 2003). Also, NPY was shown to inhibit glutamate release onto hippocampal pyramidal cells in slice preparations from human epileptic foci (Vezzani et al. 1999). In lack of in vitro studies, it is unclear how NPY neurons may affect the firing properties of cholinergic neurons. However, considering their opposite firing relation to EEG activation as compared to that of cholinergic neurons (Duque et al. 2000), the possibility that they contain GABA, and/or somatostatin, and the conditions required for release of neuropeptides (Hökfelt 1991), it is likely that during synchronized EEG epochs, when NPY neurons show burst firing (Duque et al. 2000), an increased release of NPY could result in a pronounced modulation of GABAergic-cholinergic transmission at least in the ventral pallidum where cholinergic cell bodies are richly innervated by GABAergic terminals (Zaborszky et al. 1986). A similar scenario has been postulated for the action of somatostatin that has recently been shown to inhibit presynaptically both GABA and glutamate release onto rat BF cholinergic neurons (Momiyama and Zaborszky 2006).

Concluding remarks

The 3D reconstruction of electrophysiologically and neurochemically identified neurons in the BF is an important step towards understanding the functional circuitry of this brain area. Future modeling studies should incorporate the morphological details described along with the specific active dendritic conductances for analyzing their role in synaptic integration. Knowledge of precise synaptic distributions and recordings of both the pre- and postsynaptic neurons would further our understanding of the computational roles of NPY and cholinergic neurons within their functional neural circuits and how the outputs of NPY neurons affect action potential generation in principal BF cells including cholinergic and GABAergic projection neurons.

Acknowledgments This work was supported by: NIH NS23945, NS34865, NS39600, R25 GM60826, and NSF 9413198. The authors wish to acknowledge that some of the neurons analyzed in this study were juxtacellularly labeled in cooperation with Dr. B. Balatoni. Plastic embedding of sections was done by Mrs. Erzsebet Rommer.

References

Allen YS, Adrian TE, Allen JM, Tatemoto K, Crow TJ, Bloom SR, Polak JM (1983) Neuropeptide Y distribution in the rat brain. Science 221:877–879

Alonso A, Khateb A, Fort P, Jones BE, Muhlethaler M (1996) Differential oscillatory properties of cholinergic and noncholinergic nucleus basalis neurons in guinea pig brain slice. Eur J Neurosci 8:169–182

Aoki C, Pickel VM (1989) Neuropeptide Y in the cerebral cortex and the caudate-putamen nuclei: ultrastructural basis for interactions with GABAergic and non-GABAergic neurons. J Neurosci 9:4333–4354

Arendt T, Zvegintseva HG, Leontovich TA (1986) Dendritic changes in the basal nucleus of Meynert and in the diagonal band nucleus in Alzheimer's disease—a quantitative Golgi investigation. Neuroscience 19:1265–1278

Bartus RT, Flicker C, Dean RL, Fisher S, Pontecorvo M, Figueiredo J (1986) Behavioral and biochemical effects of nucleus basalis magnocellularis lesions: implications and possible relevance to understanding or treating Alzheimer's disease. Prog Brain Res 70:345–361

Bengtson CP, Osborne PB (2000) Electrophysiological properties of cholinergic and noncholinergic neurons in the ventral pallidal region of the nucleus basalis in rat brain slices. J Neurophysiol 83:2649–2660

Bialowas J, Frotscher M, (1987) Choline acetyltransferase-immunoreactive neurons and terminals in the rat septal complex: a combined light and electron microscopic study. J Comp Neurol 259:298–307

Book AA, Wiley RG, Schweitzer JB (1994) 192 IgG-saporin: I. Specific lethality for cholinergic neurons in the basal forebrain of the rat. J Neuropathol Exp Neurol 53:95–102

Brashear HR, Zaborszky L, Heimer L (1986) Distribution of GABAergic and cholinergic neurons in the rat diagonal band. Neuroscience 17:439–451

Brauer K, Schober W, Werner L, Winkelmann E, Lungwitz W, Hajdu F (1988) Neurons in the basal forebrain complex of the rat: a Golgi study. J Hirnforsch 29:43–71

Brauer K, Seeger G, Hartig W, Rossner S, Poethke R, Kacza J, Schliebs R, Bruckner G, Bigl V (1998) Electron microscopic evidence for a cholinergic innervation of GABAergic parvalbumin-immunoreactive neurons in the rat medial septum. J Neurosci Res 54:248–253

Carnevale NT, Tsai KY, Claiborne BJ, Brown TH (1997) Comparative electrotonic analysis of three classes of rat hippocampal neurons. J Neurophysiol 78:703–720

Chen G, van den Pol AN (1996) Multiple NPY receptors coexist in pre- and postsynaptic sites: inhibition of GABA release in isolated self-innervating SCN neurons. J Neurosci 16:7711–7724

Chronwall BM, DiMaggio DA, Massari VJ, Pickel VM, Ruggiero DA, O'Donohue TL (1985) The anatomy of neuropeptide-Y-containing neurons in rat brain. Neuroscience 15:1159–1181

Csillik B, Rakic P, Knyihar-Csillik E (1998) Peptidergic innervation and the nicotinic acetylcholine receptor in the primate basal nucleus. Eur J Neurosci 10:573–585

Dani JA (2001) Overview of nicotinic receptors and their roles in the central nervous system. Biol Psychiatry 49:166–174

Davies P, Maloney AJ (1976) Selective loss of central cholinergic neurons in Alzheimer's disease [letter]. Lancet 2:1403

de Quidt ME, Emson PC (1986a) Distribution of neuropeptide Y-like immunoreactivity in the rat central nervous system-II. Immunohistochemical analysis. Neuroscience 18:545–618

de Quidt ME, Emson PC (1986b) Distribution of neuropeptide Y-like immunoreactivity in the rat central nervous system-I. Radioimmunoassay and chromatographic characterisation. Neuroscience 18:527–543

Detari L (2000) Tonic and phasic influence of basal forebrain unit activity on the cortical EEG. Behav Brain Res 115:159–170

Detari L, Vanderwolf CH (1987) Activity of identified cortically projecting and other basal forebrain neurones during large slow waves and cortical activation in anaesthetized rats. Brain Res 437:1–8

Detari L, Rasmusson DD, Semba K (1999) The role of basal forebrain neurons in tonic and phasic activation of the cerebral cortex. Prog Neurobiol 58:249–277

Dringenberg HC, Vanderwolf CH (1998) Involvement of direct and indirect pathways in electrocorticographic activation. Neurosci Biobehav Rev 22:243–257

Duque A, Zaborszky L (2006) Juxtacellular labeling of individual neurons in vivo: from electrophysiology to synaptology. In: Zaborszky L, Wouterlood FG, Lanciego JL (eds) Neuroanatomical tract-tracing 3 molecules, neurons, and systems. Springer, New York, pp 197–236

Duque A, Balatoni B, Detari L, Zaborszky L (2000) EEG correlation of the discharge properties of identified neurons in the basal forebrain. J Neurophysiol 84:1627–1635

Edvinsson L, Minthon L, Ekman R, Gustafson L (1993) Neuropeptides in cerebrospinal fluid of patients with Alzheimer's disease and dementia with frontotemporal lobe degeneration. Dementia 4:167–171

Fisher RS, Levine MS (1989) Transmitter cosynthesis by corticopetal basal forebrain neurons. Brain Res 491:163–168

Geula C, Mesulam MM (1994) Cholinergic systems and related neuropathological predilection patterns in Alzheimer disease. In: Terry RD, Katzman R, Bick KL (eds) Alzheimer disease. Raven, New York, pp 263–291

Gotti C, Fornasari D, Clementi F (1997) Human neuronal nicotinic receptors. Prog Neurobiol 53:199–237

Gritti I, Manns ID, Mainville L, Jones BE (2003) Parvalbumin, calbindin, or calretinin in cortically projecting and GABAergic, cholinergic, or glutamatergic basal forebrain neurons of the rat. J Comp Neurol 458:11–31

Hajszan T, Zaborszky L (2002) Direct catecholaminergic-cholinergic interactions in the basal forebrain. III. Adrenergic innervation of choline acetyltransferase-containing neurons in the rat. J Comp Neurol 449:141–157

Heimer L, de Olmos J, Alheid GF, Zaborszky L (1991) ''Perestroika'' in the basal forebrain: opening the border between neurology and psychiatry. Prog Brain Res 87:109–165

Hökfelt T (1991) Neuropeptides in perspective: the last ten years. Neuron 7:867–879

Horikawa K, Armstrong WE (1988) A versatile means of intracellular labeling: injection of biocytin and its detection with avidin conjugates. J Neurosci Methods 25:1–11

Hur EE, Zaborszky L (2005) Vglut2 afferents to the medial prefrontal and primary somatosensory cortices: a combined retrograde tracing in situ hybridization. J Comp Neurol 483(3):351–73

Jaeger D (2001) Accurate reconstruction of neuronal morphology. In: De Schutter E (ed) Computational neuroscience: realistic modeling for experimentalists. Lewis, Boca Raton, pp 159–178

Jones BE, Muhlethaler M (1999) Cholinergic and GABAergic neurons of the basal forebrain: role in cortical activation. In: Lydic R, Baghdoyan HA (eds) Handbook of behavioral state control—cellular and molecular mechanisms. CRC, Boca Raton, pp 213–234

Kaspirzhny AV, Gogan P, Horcholle-Bossavit G, Tyc-Dumont S (2002) Neuronal morphology data bases: morphological noise and assessment of data quality. Network 13:357–380

Khateb A, Muhlethaler M, Alonso A, Serafin M, Mainville L, Jones BE (1992) Cholinergic nucleus basalis neurons display the capacity for rhythmic bursting activity mediated by low-threshold calcium spikes. Neuroscience 51:489–494

Khateb A, Fort P, Williams S, Serafin M, Jones BE, Muhlethaler M (1997) Modulation of cholinergic nucleus basalis neurons by acetylcholine and N-methyl-D-aspartate. Neuroscience 81:47–55

Khateb A, Fort P, Williams S, Serafin M, Muhlethaler M, Jones BE (1998) GABAergic input to cholinergic nucleus basalis neurons. Neuroscience 86:937–947

Köhler C, Eriksson L, Davies S, Chan-Palay V (1986) Neuropeptide Y innervation of the hippocampal region in the rat and monkey brain. J Comp Neurol 244:384–400

Krichmar JL, Nasuto SJ, Scorcioni R, Washington SD, Ascoli GA (2002) Effects of dendritic morphology on CA3 pyramidal cell electrophysiology: a simulation study. Brain Res 941:11–28

Leontovich TA, Zhukova GP (1963) The specificity of the neuronal structure and topography of the reticular formation in the brain and spinal cord of carnivora. J Comp Neurol 121:347–379

Li Y, Brewer D, Burke RE, Ascoli GA (2005) Developmental changes in spinal motoneuron dendrites in neonatal mice. J Comp Neurol 483:304–317

Manns ID, Alonso A, Jones BE (2000) Discharge properties of juxtacellularly labeled and immunohistochemically identified cholinergic basal forebrain neurons recorded in association with the electroencephalogram in anesthetized rats. J Neurosci 20:1505–1518

Metcalf RH, Boegman RJ (1989) Release of acetylcholine from tissue slices of the rat nucleus basalis magnocellularis. J Neurochem 52:1143–1148

Metcalf RH, Boegman RJ, Riopelle RJ, Ludwin SK (1988) The release of endogenous acetylcholine from the medial septum/diagonal band of rat brain. Neurosci Lett 93:85–90

Millhouse OE (1986) Pallidal neurons in the rat. J Comp Neurol 254:209–227

Minthon L, Edvinsson L, Gustafson L (1996) Correlation between clinical characteristics and cerebrospinal fluid neuropeptide Y levels in dementia of the Alzheimer type and frontotemporal dementia. Alzheimer Dis Assoc Disord 10:197–203

Momiyama T, Zaborszky L (2006) Somatostatin presynaptically inhibits both GABA and glutamate release onto rat basal forebrain cholinergic neurons. J Neurophysiol 96:686–694

Mosca KF, Duque A, Detari L, Noszek A, Rommer E, Zaborszky L (2005) Postsynaptic target of electrophysiologically identified NPY axons in the rat basal forebrain. Program No. 936.1. SFN Abstracts. Washington DC, Online

Nishimura LM, Boegman RJ (1990) N-methyl-D-aspartate-evoked release of acetylcholine from the medial septum/diagonal band of rat brain. Neurosci Lett 115:259–264

Nunez A (1996) Unit activity of rat basal forebrain neurons: relationship to cortical activity. Neuroscience 72:757–766

Pang K, Tepper JM, Zaborszky L (1998) Morphological and electrophysiological characteristics of noncholinergic basal forebrain neurons. J Comp Neurol 394:186–204

Picciotto MR, Caldarone BJ, King SL, Zachariou V (2000) Nicotinic receptors in the brain. Links between molecular biology and behavior. Neuropsychopharmacology 22:451–465

Pinault D (1994) Golgi-like labeling of a single neuron recorded extracellularly. Neurosci Lett 170:255–260

Pinault D (1996) A novel single-cell staining procedure performed in vivo under electrophysiological control: morpho-functional features of juxtacellularly labeled thalamic cells and other central neurons with biocytin or neurobiotin. J Neurosci Methods 65:113–136

Poirazi P, Brannon T, Mel BW (2003) Arithmetic of subthreshold synaptic summation in a model CA1 pyramidal cell. Neuron 37:977–987

Ramon-Moliner E (1962) An attempt at classifying nerve cells on the basis of their dendritic patterns. J Comp Neurol 119:211–227

Ramon-Moliner E, Nauta WJ (1966) The isodendritic core of the brain stem. J Comp Neurol 126:311–336

Reiner PB, Semba K, Fibiger HC, McGeer EG (1987) Physiological evidence for subpopulations of cortically projecting basal forebrain neurons in the anesthetized rat. Neuroscience 20:629–636

Sarter M, Bruno JP (1999) Abnormal regulation of corticopetal cholinergic neurons and impaired information processing in neuropsychiatric disorders. Trends Neurosci 22:67–74

Sarter M, Parikh V (2005) Choline transporters, cholinergic transmission and cognition. Nat Rev Neurosci 6:48–56

Schaefer AT, Larkum ME, Sakmann B, Roth A (2003) Coincidence detection in pyramidal neurons is tuned by their dendritic branching pattern. J Neurophysiol 89:3143–3154

Scheibel ME, Scheibel AB (1961) On circuit patterns of the brain stem reticular core. Ann N Y Acad Sci 89:857–865

Scorcioni RE, Ascoli GA (2001) Algorithmic extraction of morphological statistics from electronic archives of neuroanatomy. Lect Notes Comp Sci 2084:30–37

Scorcioni R, Lazarewicz MT, Ascoli GA (2004) Quantitative morphometry of hippocampal pyramidal cells: differences between anatomical classes and reconstructing laboratories. J Comp Neurol 473:177–193

Semba K, Reiner PB, McGeer EG, Fibiger HC (1987) Morphology of cortically projecting basal forebrain neurons in the rat as revealed by intracellular iontophoresis of horseradish peroxidase. Neuroscience 20:637–651

Sim JA, Griffith WH (1996) Muscarinic inhibition of glutamatergic transmissions onto rat magnocellular basal forebrain neurons in a thin-slice preparation. Eur J Neurosci 8:880–891

Smiley JF, Levey AI, Mesulam MM (1999a) m2 muscarinic receptor immunolocalization in cholinergic cells of the monkey basal forebrain and striatum. Neuroscience 90:803–814

Smiley JF, Subramanian M, Mesulam MM (1999b) Monoaminergic-cholinergic interactions in the primate basal forebrain. Neuroscience 93:817–829

Sun QQ, Akk G, Huguenard JR, Prince DA (2001) Differential regulation of GABA release and neuronal excitability mediated by neuropeptide Y1 and Y2 receptors in rat thalamic neurons. J Physiol 531:81–94

Sun QQ, Baraban SC, Prince DA, Huguenard JR (2003) Target-specific neuropeptide Y-ergic synaptic inhibition and its network consequences within the mammalian thalamus. J Neurosci 23:9639–9649

Surkis A, Taylor B, Peskin CS, Leonard CS (1996) Quantitative morphology of physiologically identified and intracellularly labeled neurons from the guinea-pig laterodorsal tegmental nucleus in vitro. Neuroscience 74:375–392

Toth A, Zaborszky L, Detari L (2005) EEG effect of basal forebrain neuropeptide Y administration in urethane anaesthetized rats. Brain Res Bull 66:37–42

Valverde F (1961a) A new type of cell in the lateral reticular formation of the brain stem. J Comp Neurol 117:189–195

Valverde F (1961b) Reticular formation of the pons and medulla oblongata. A Golgi study. J Comp Neurol 116:71–99

Vetter P, Roth A, Hausser M (2001) Propagation of action potentials in dendrites depends on dendritic morphology. J Neurophysiol 85:926–937

Vezzani A, Sperk G, Colmers WF (1999) Neuropeptide Y: emerging evidence for a functional role in seizure modulation. Trends Neurosci 22:25–30

Vilaro MT, Palacios JM, Mengod G (1994) Multiplicity of muscarinic autoreceptor subtypes? Comparison of the distribution of cholinergic cells and cells containing mRNA for five subtypes of muscarinic receptors in the rat brain. Brain Res Mol Brain Res 21:30–46

Voytko ML, Olton DS, Richardson RT, Gorman LK, Tobin JR, Price DL (1994) Basal forebrain lesions in monkeys disrupt attention but not learning and memory [published erratum appears in J Neurosci 1995 Mar;15(3 Pt 2):following table of contents]. J Neurosci 14:167–186

Walker LC, Koliatsos VE, Kitt CA, Richardson RT, Rokaeus A, Price DL (1989a) Peptidergic neurons in the basal forebrain magnocellular complex of the rhesus monkey. J Comp Neurol 280:272–282

Walker LC, Price DL, Young WS (1989b) GABAergic neurons in the primate basal forebrain magnocellular complex. Brain Res 499:188–192

Whitehouse PJ, Price DL, Struble RG, Clark AW, Coyle JT, Delon MR (1982) Alzheimer's disease and senile dementia: loss of neurons in the basal forebrain. Science 215:1237–1239

Wolak ML, DeJoseph MR, Cator AD, Mokashi AS, Brownfield MS, Urban JH (2003) Comparative distribution of neuropeptide Y Y1 and Y5 receptors in the rat brain by using immunohistochemistry. J Comp Neurol 464:285–311

Wu M, Shanabrough M, Leranth C, Alreja M (2000) Cholinergic excitation of septohippocampal GABA but not cholinergic neurons: implications for learning and memory. J Neurosci 20:3900–3908

Yu MC, Luo CB, Long L, Yew DT (1993) An immunohistochemical study of neuropeptide Y positive sites in the developing human hippocampal formation. Brain Res Dev Brain Res 72:277–281

Zaborszky L, Cullinan WE (1996) Direct catecholaminergic-cholinergic interactions in the basal forebrain. I. Dopamine-beta-hydroxylase- and tyrosine hydroxylase input to cholinergic neurons. J Comp Neurol 374:535–554

Zaborszky L, Duque A (2000) Local synaptic connections of basal forebrain neurons. Behav Brain Res 115:143–158

Zaborszky L, Duque A (2003) Sleep–wake mechanisms and basal forebrain circuitry. Front Biosci 8:d1146–d1169. [PubMed#:12957822] http://www.bioscience.org/

Zaborszky L, Heimer L, Eckenstein F, Leranth C (1986) GABAergic input to cholinergic forebrain neurons: an ultrastructural study using retrograde tracing of HRP and double immunolabeling. J Comp Neurol 250:282–295

Zaborszky L, Pang K, Somogyi J, Nadasdy Z, Kallo I (1999) The basal forebrain corticopetal system revisited. Ann N Y Acad Sci 877:339–367

Zaborszky L, Csordas A, Duque A, Somogy J, Nadasdy Z (2002) Computational anatomical analysis of the basal forebrain corticopetal system. In: Ascoli G (ed) Computational neuroanatomy: principles and methods. Humana, Totowa, pp 171–197

Zador AM, Agmon-Snir H, Segev I (1995) The morphoelectrotonic transform: a graphical approach to dendritic function. J Neurosci 15:1669–1682